Supporting Information

4,5-Diazido-6-nitropyridazin-3(2*H*)-one: A Versatile Nitrogen-Rich Compound for Multifaceted Energetic Applications

Sonali Kukreja, Abhishek Kumar Yadav and Srinivas Dharavath*

Energetic Materials Laboratory, Department of Chemistry, Indian Institute of Technology Kanpur, Kanpur-208016, Uttar Pradesh, India. E-mail: srinivasd@iitk.ac.in

Table of Contents

Experimental Section:

Caution! The compounds in this work are energetic materials that could potentially explode under certain conditions (e.g., impact, friction, or electric discharge). Appropriate safety precautions, such as the use of shields in a fume hood and personal protection equipment (safety glasses, face shields, ear plugs, as well as gloves) should always be taken when handling these materials.

General. All reagents were purchased from AKSci or TCI or Merck in analytical grade and were used as supplied. ^{1}H, and $^{13}C\{^{1}H\}$ spectra were recorded using JEOL DELTA (ECS) 500 (^{1}H, 500 MHz) and $^{13}C\{^{1}H\}$ NMR (126 MHz, DMSOd6) nuclear magnetic resonance spectrometer. Chemical shifts for ^{1}H NMR and $^{13}C\{^{1}H\}$ NMR spectra are given with respect to external $(CH_3)_4Si$ (^{1}H and ^{13}C). [D6] DMSO was used as a locking solvent unless otherwise stated. IR spectra were recorded using Zn-Se pellets with a ECO-ATR spectrometer (Bruker Alpha II). A single crystal of suitable dimensions was used for data collection. Diffraction intensities were collected on a Bruker APEX-II CCD diffractometer, with graphite-monochromated Mo Kα (0.71073 Å) radiation at 100(2) K. The structure was solved with the ShelXT[1] solution program using dual methods and by using Olex2. The model was refined with ShelXL[2] using full matrix least squares minimisation on $\boldsymbol{F^2}$. The thermal ellipsoids and packing diagrams of X-ray structures in the main article and supplementary material are plotted using Olex 2 software.[3] Density was determined at room temperature by employing Anton Par Ultra5000 gas pycnometer. Mass data was recorded using LC-MS (ESI)-Q-TOF (Agilent 6546) mass spectrometer. Decomposition temperatures (onset) were recorded using a dry nitrogen gas purge and a heating rate of 10 °C min^{-1} on a thermogravimetric differential scanning calorimeter (TGA-DSC (SDT-650)). Impact and friction sensitivity measurements were made using a standard BAM fall hammer and a BAM friction tester.

Synthesis of 4,5-dichloro-6-nitropyridazin-3(2H)-one (1): Compound **1** was synthesized according to the literature method.[4]

Synthesis of 4,5-diazido-6-nitropyridazin-3(2H)-one (2): Compound **1** (1 g, 4.76 mmol) was dissolved in a 1:1 mixture of acetone and water. Sodium azide was then added portionwise to the reaction mixture, which was subsequently heated at 50 °C for 12 hours, resulting in a clear solution. After completion, the solvents were evaporated, and the resulting residue was washed with water and filtered to afford Compound **2** in 80% yield. (0.850 g, 3.81 mmol) ^{1}H NMR (500 MHz, DMSO-d6): δ 13.95 (s, 1H). $^{13}C\{^{1}H\}$ NMR (126 MHz, DMSO-d6) δ 158.1, 144.7

131.6, 121.6 . IR (ATR ZnSe): 3194.7, 3131.4, 3024.1, 2884.4, 2829.1, 2125.6, 1644.9, 1588.6, 1539.2, 1469.1, 1358.4, 1296.9, 1236.2, 881.3,819.1, 755.5, 655.0 cm^{-1}. Elemental Analysis Calcd for $C_4HN_9O_3$: C, 21.53 ; H, 0.45 ; N, 56.50. Found: C, 21.35; H, 0.26; N, 56.30. HRMS (ESI-QTOF) m/z: $[M - 2N_2 - H]^-$ Calcd for $C_4N_5O_3$: 166.0007; Found: 166.0011.

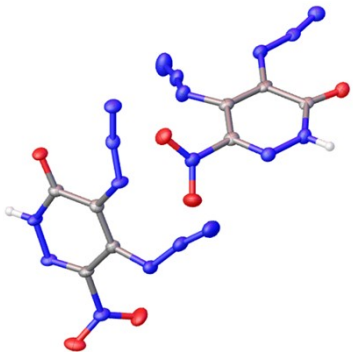

Figure S1: Crystal Structure of **2**.

Table S1. Crystal data and structure refinement for Compound 2.

CCDC No.	2478396
Empirical formula	$C_8H_2N_{18}O_6$
Formula weight	446.28
Temperature/K	100
Crystal system	triclinic
Space group	P-1
a/Å	6.479(3)
b/Å	11.334(5)
c/Å	11.614(5)
α/°	105.371(9)
β/°	96.160(10)
γ/°	97.443(10)
Volume/Å3	806.4(6)
Z	2
ρcalcg/cm3	1.838
μ/mm-1	0.159
F(000)	448.0
Crystal size/mm3	0.13 × 0.12 × 0.11
Radiation	MoKα (λ = 0.71073)

2Θ range for data collection/°	4.466 to 57.684
Index ranges	-8 ≤ h ≤ 8, -15 ≤ k ≤ 15, -15 ≤ l ≤ 15
Reflections collected	11044
Independent reflections	4101 [Rint = 0.0711, Rsigma = 0.0827]
Data/restraints/parameters	4101/0/289
Goodness-of-fit on F2	1.023
Final R indexes [I>=2σ (I)]	R1 = 0.0645, wR2 = 0.1486
Final R indexes [all data]	R1 = 0.1084, wR2 = 0.1730
Largest diff. peak/hole / e Å^{-3}	0.44/-0.50

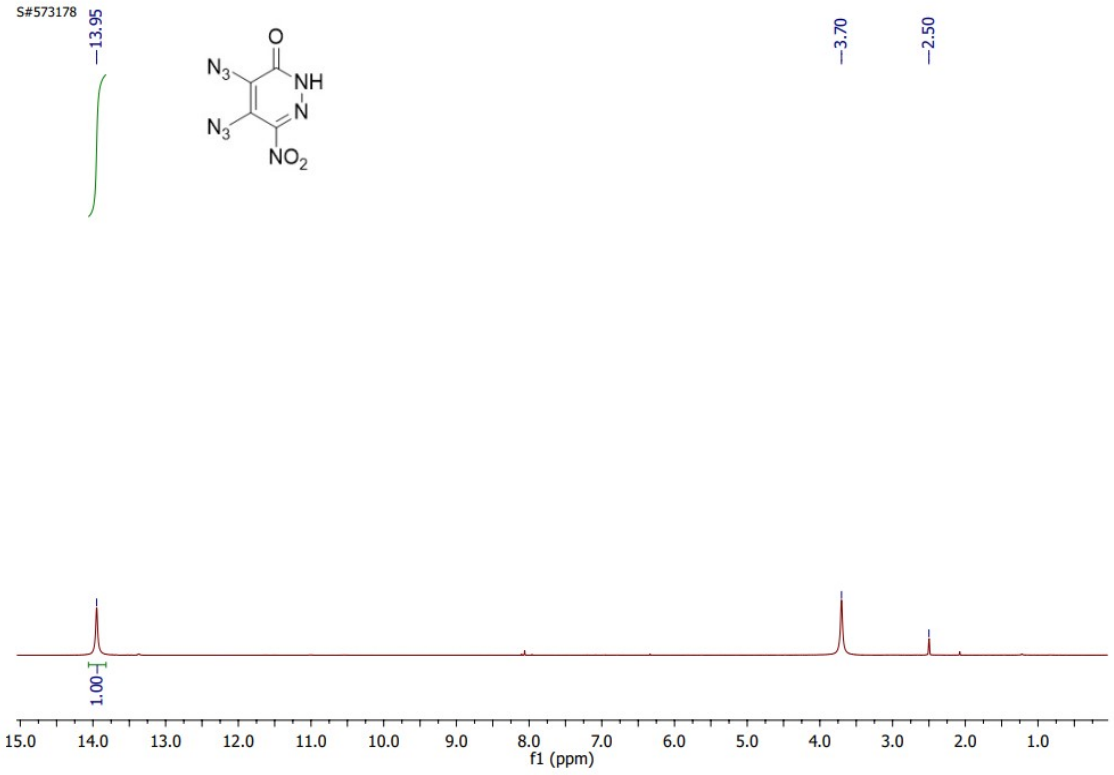

Figure S2: ^{1}H NMR Spectrum of Compound 2 (recorded in DMSO-d6; 500 MHz).

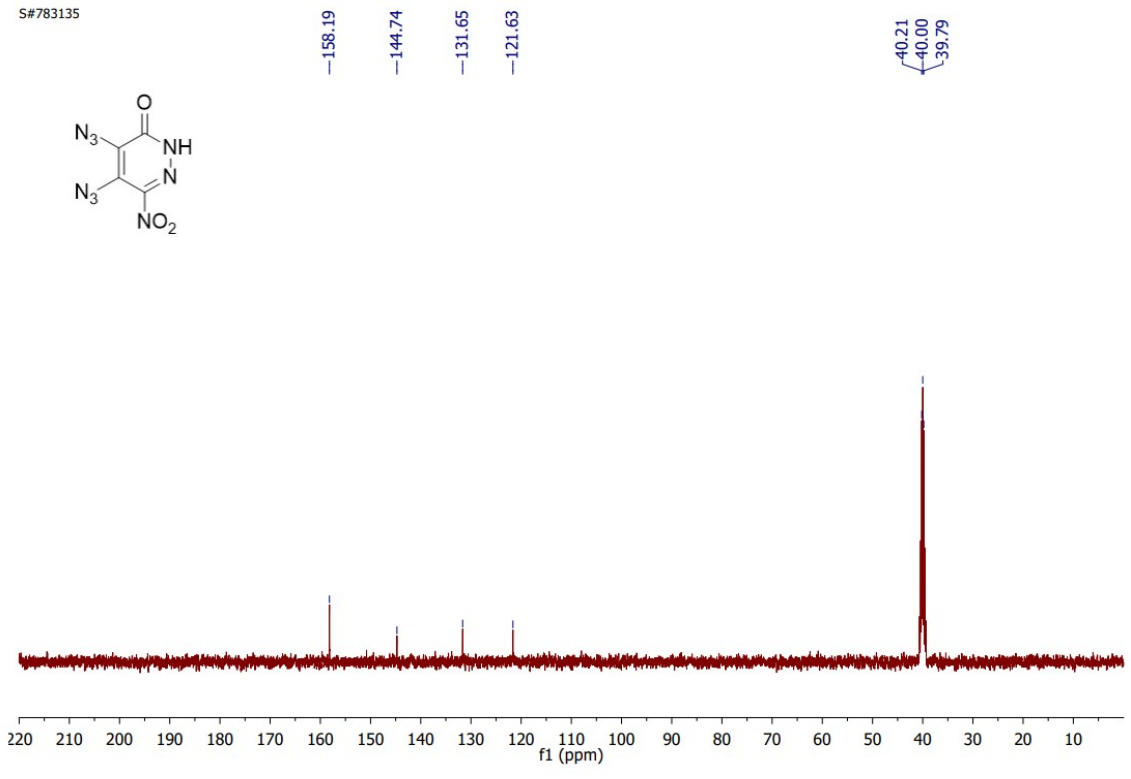

Figure S3: $^{13}C\{^{1}H\}$ NMR Spectrum of Compound 2 (recorded in DMSO-d6; 126 MHz).

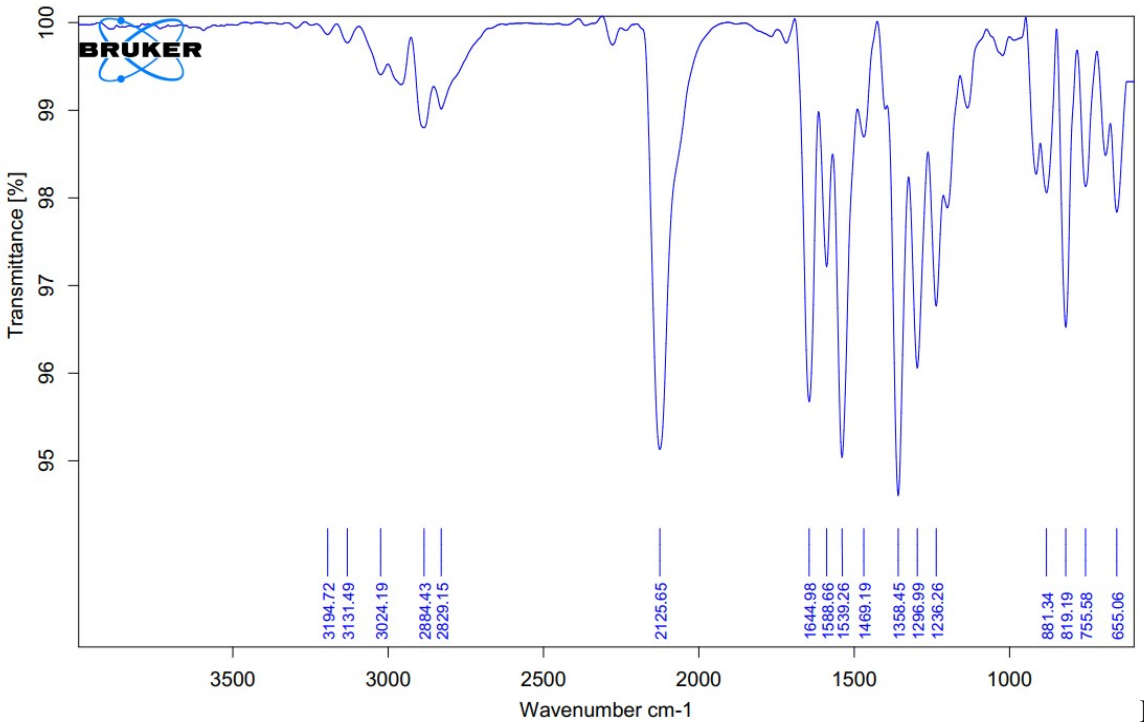

Figure S4: IR Spectrum of Compound 2.

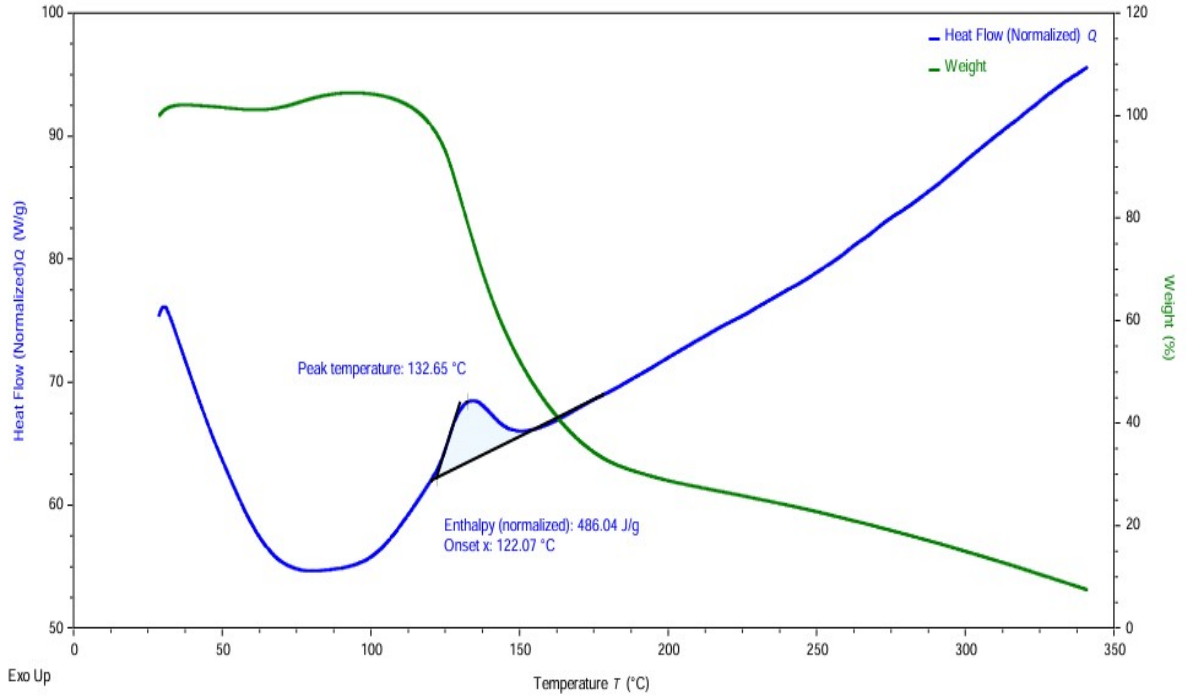

Figure S5: DSC Plot of Compound 2 at Heating rate 10 ^{o}C min^{-1}.

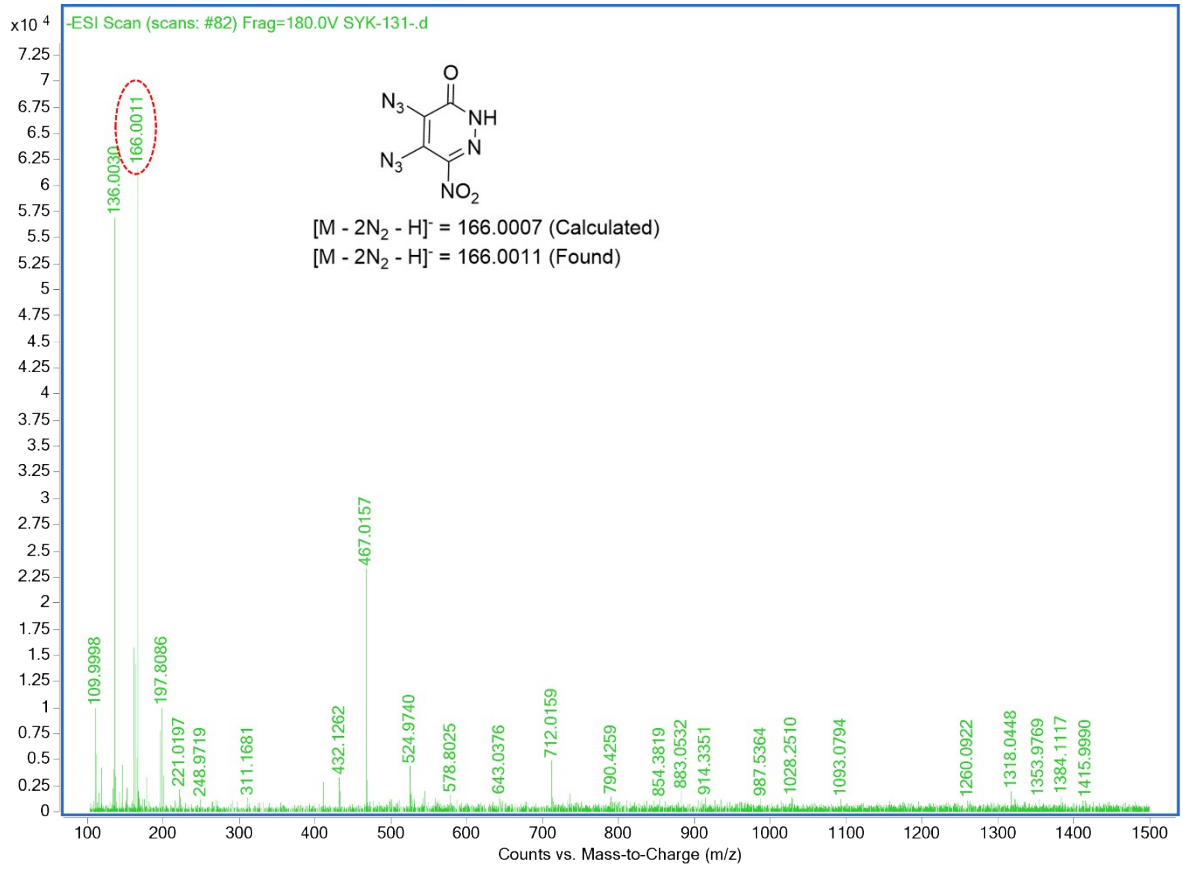

Figure S6: Mass spectrum of 2.

Table S2: Physicochemical properties of compound 2

Compound	T_d [a] [°C]	ρ[b] [g cm^{-3}]	HOF[c] [kJ mol^{-1}]	DP[d] [GPa]	VOD[e] [m s^{-1}]	IS[f] [J]	FS[g] [N]
2	122	1.80	220	24.17	7967	5	120

[a]Onset decomposition temperature (DSC, 10 °C/min), [b]Pycnometer density at 25 °C, [c]Computed heat of formation (calculated with Gaussian 09 program); [d]Detonation pressure calculated with EXPLO5 v7.01.01; [e]Detonation velocity calculated with EXPLO5 v7.01.01; [f]Impact sensitivity; [g]Friction sensitivity

Hirshfeld surface analysis of compound 2

Hirshfeld surface analysis and two-dimensional (2D) fingerprint plots were utilized to gain deeper insights into the molecular stability and sensitivity of compound **2** using Crystal Explorer Software as shown in **Figure S7**. On the Hirshfeld surface, the intense red regions, indicative of significant close contacts are predominantly located on the lateral sides of the molecular plates rather than the front faces. This distribution suggests that intermolecular interactions primarily involve peripheral atoms, particularly hydrogen and nitrogen, which envelop the molecular framework. As shown in **Figure S7 (c)**, the Hirshfeld surface analysis quantifies the relative contributions of various intermolecular interactions in compound **2**. The N···H (7.7%) and O···H (5.6%) interactions play a stabilizing role by facilitating hydrogen bonding, which enhances the stability of the compound. Additionally, N···O (41.3%) C···N (9.1%) and O···C (6.3%) contacts support π–π stacking and n→π* interactions, further strengthening the intermolecular framework. The most prominent contacts are and N···N and O···O contacts, comprising 26.0% and 3% respectively, of the total surface interactions. These contacts are typically associated with destabilizing effects and contribute to the compound's heightened sensitivity and low thermal stability.

Collectively, the high prevalence of N···N contacts aligns with the observed sensitivity of compound **2**, while stabilizing contributions from N···H, O···H, C···N, N···O and O···C interactions help to maintain structural integrity. This comprehensive interaction profile offers valuable insight into the delicate interplay between sensitivity and stability in the structure of compound **2**.

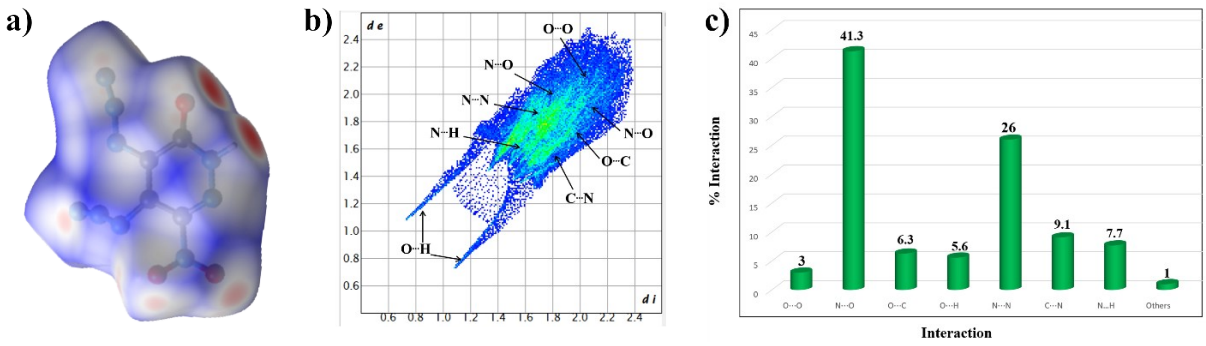

Figure S7: (a) Hirshfeld surface of **2**. (b) 2D fingerprint plots in the crystal stacking for **2**. (c) bar Graph showing % contribution of individual atomic contacts to the Hirshfeld surface.

Burning Test of Compound 2 with Ammonium Nitrate (AN)

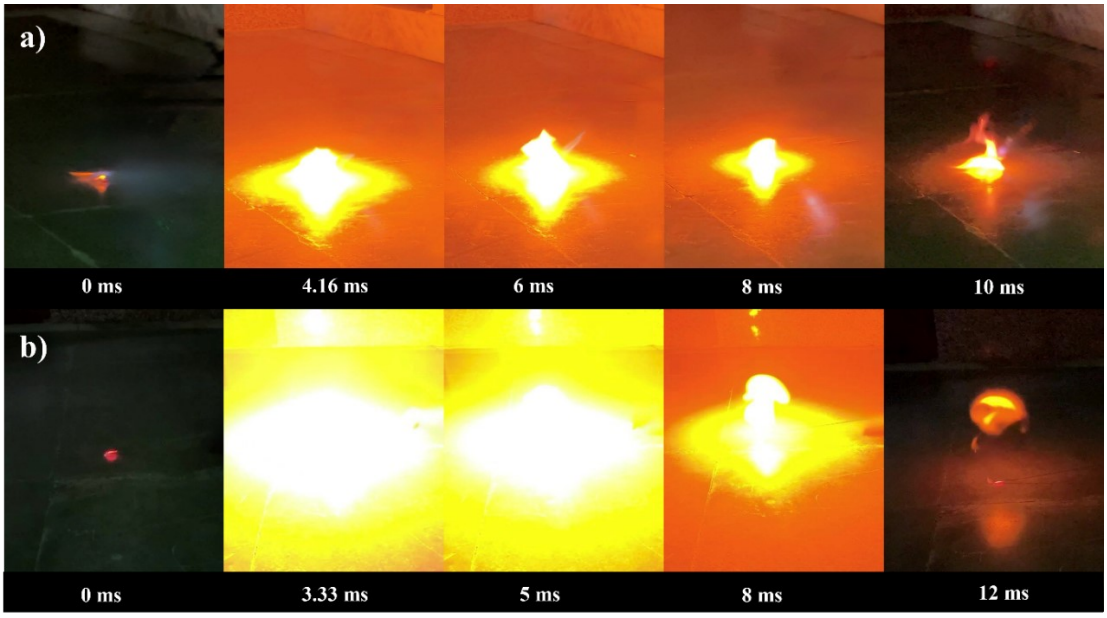

Figure S8. a) Ignition test for compound **2**. b) Ignition test for formulation of compound **2** and AN.

Burning Images of pure AN

Figure S9: Before and After images of burning of pure AN.

Burning Test of Compound 2 with Ammonium perchlorate (AP)

To evaluate the burning behaviour and compatibility of the synthesized compound **2** with ammonium perchlorate (AP), a formulation was prepared in a 1:2 molar ratio of compound **2** to AP, ensuring a zero-oxygen balance with respect to carbon dioxide. The recorded ignition delay time for the formulation was 3.1 ms, notably shorter than that of pure compound **2**, which exhibited an ignition delay of 4.16 ms. Additionally, the total burning duration increased to 13.5 ms compared to 10 ms for pure compound **2**.

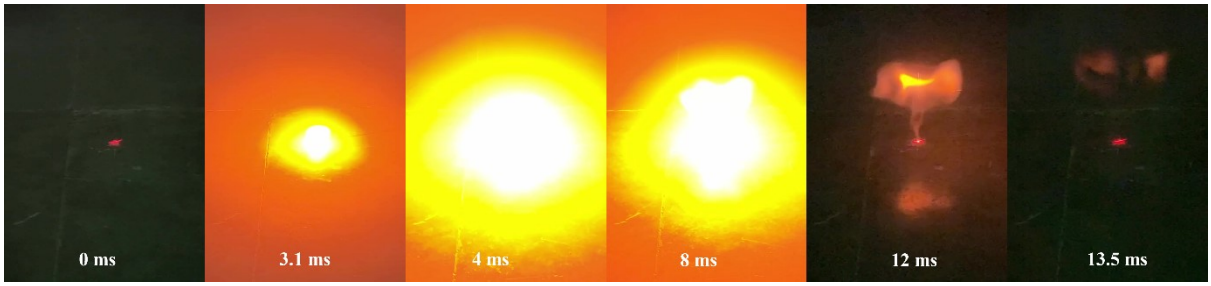

Figure S10: Ignition test for formulation of compound **2** and AP.

Stability of the Propellant Formulations

In order to robustly evaluate the long-term chemical stability and potential interactions of compound **2** and AN / AP formulations, a vacuum–thermal stability assessment was performed using an in-house high-vacuum system. Formulations of AN/ AP with Compound **2** were heated at 70 °C under reduced pressure for 8 h. Fourier-transform infrared (FT-IR) spectra were recorded before and after the vacuum–thermal treatment. The post-treatment spectra were essentially identical to the corresponding pre-treatment spectra, with no appearance, disappearance, or shift of characteristic absorption bands as depicted in **Figures S11- S12**. These results confirm that compound **2** remains chemically intact and does not undergo degradation or adverse interactions with AN or AP under prolonged thermal exposure in vacuum. Hence these results provide meaningful evidence supporting the chemical compatibility and thermal stability of the synthesized propellant formulations.

Compound **2** / AN Formulation

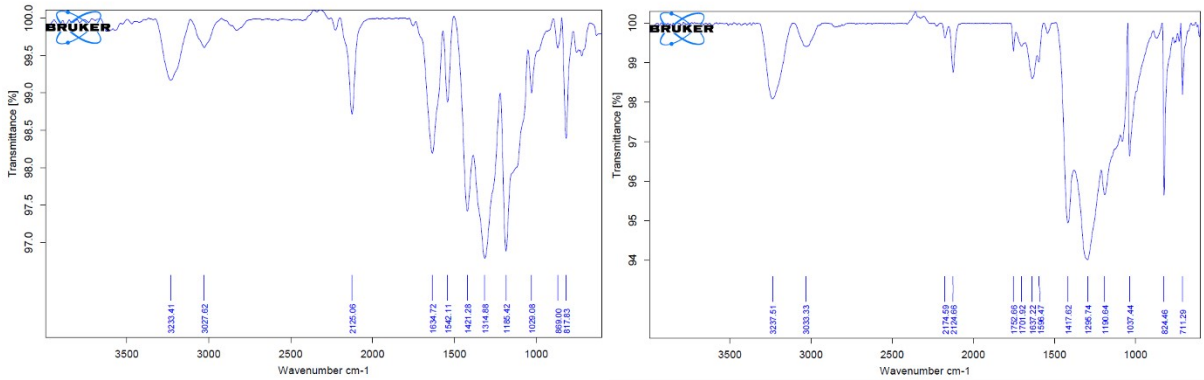

Before vacuum- thermal treatment

After vacuum- thermal treatment

Figure S11. IR spectra of compound **2** / AN formulation before and after the vacuum- thermal treatment.

Compound **2** / AP Formulation

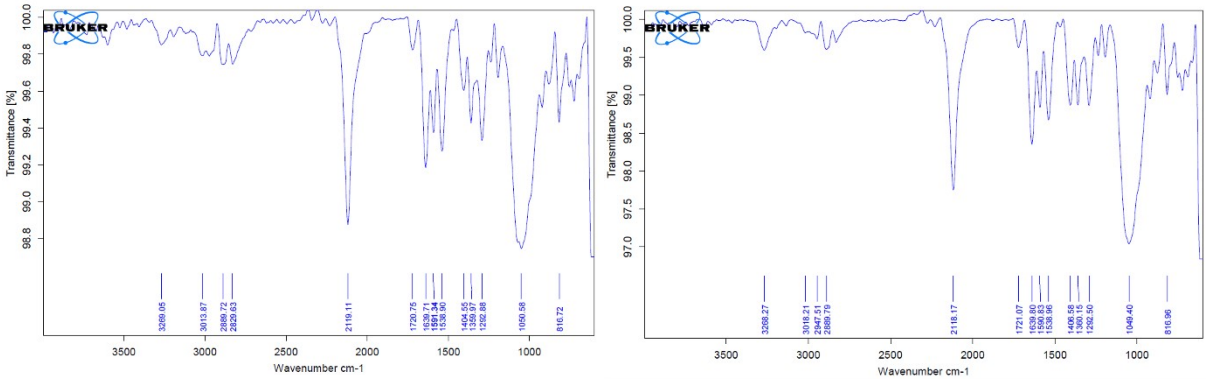

Before vacuum- thermal treatment

After vacuum- thermal treatment

Figure S12. IR spectra of compound **2** / AP formulation before and after the vacuum- thermal treatment.

Specific Impulse calculations

To assess the suitability of compound **2** as a potential energetic component for solid rocket propellants, comparative performance calculations were performed by replacing established high-energy secondary explosives with compound **2** in similar propellant formulations. As presented in **Table S3**, formulations containing RDX and HMX show higher specific impulse values (274 s each) than that of the formulation incorporating compound **2**. The relatively lower specific impulse observed for compound **2** can be rationalized by its intrinsically lower energetic output, as it functions as a less energetic primary explosive, in contrast to the more energetic secondary explosives RDX and HMX. Accordingly, these results

place the performance of compound **2** in an appropriate context and indicate its potential utility as an energetic filler in propellant formulations.

Table S3: EXPLO5 calculation results using Klapötke and Suceska method[5] for various high-energy composite (HEC) propellant formulations.

High Energy Component	**RDX**	**HMX**	**Compound 2**
Formulation	10 % GAP, 15 % NG, 18% Al, 45% RDX, 12% AP	10 % GAP, 15 % NG, 18% Al, 45% HMX, 12% AP	10 % GAP, 15 % NG, 18% Al, 34% **2**, 23 % AP
Oxygen balance [%]	-33%	-33%	-33%
Specific Impulse [s]	274	274	254
Isochoric combustion temperature [K]	3814	3806	3485
Heat of combustion [kJ/ kg]	6110	6094	4951
Exhaust Velocity [m / sec]	2694	2690	2490

Table S4: Composition of various pyrotechnic formulations.

Component (wt %)	**Fuel**	**Oxidizer/Colorant**	**Binder**
Formulation 1	Compound 2 (45%)	KNO_3 (50%)	TNT (5%)
Formulation 2	Compound 2 (45%)	$Sr(NO_3)_2$ (50%)	TNT (5%)
Formulation 3	Compound 2 (45%)	$Cu(NO_3)_2$ (50%)	TNT (5%)

Predicted Detonation By-products

Table S5: (a) Pyrotechnic Formulation 1

Product	**mol%**

N_2	52.0591
CO_2	26.7658
K_2CO_3 (s)	10.8396
H_2O	5.7698
CO	3.5027
CH_2O_2	1.0105

b) Pyrotechnic Formulation 2

Product	**mol%**
N_2	49.5721
CO_2	33.7691
CO	6.7036
$Sr(OH)_2$ (s)	6.5649
SrO (s)	3.3871

c) Pyrotechnic Formulation 3

Product	**mol%**
N_2	46.9302
CO_2	37.4909
H_2O	6.0878
Cu_2O (l)	5.2815
O_2	1.7909
NO	1.6538

SEM images and EDX data of Pyrotechnic Formulations

The surface morphologies of compound **2**, ammonium nitrate (AN), their formulated mixture and all the three pyrotechnic formulations were investigated using scanning electron microscopy (SEM), as illustrated in **Figure S13.** Prior to analysis, the samples were prepared in dry powder form and coated with a thin layer of gold to enhance image resolution. SEM imaging was performed using a ZEISS-EVO18 microscope operating at an accelerating voltage of 10 kV. As depicted in **Figure S13 (a)**, compound **2** exhibits a distinctive rod-like

morphology, characterized by uniformly dispersed nanorods with smooth surfaces and consistent dimensions, indicating well-defined crystal growth. In contrast, **Figure S13 (b)** presents a flower-like microstructure for ammonium nitrate, showcasing its unique crystalline assembly. The SEM image of the AN compound **2** formulation in **Figure S13 (c)** reveals a heterogeneous surface morphology, reflecting the integration of both components within the composite matrix. **Figure S13 (d-f)** shows the morphology of the pyrotechnic formulations 1, 2 and 3 respectively. (at magnifications of 10000X, 2000X and 1500X respectively)

Elemental mapping, obtained via Energy-Dispersive X-ray (EDX) spectroscopy, is presented in **Figure S14**. EDX analysis was employed to determine the elemental distribution within the synthesized pyrotechnic formulations. The resulting elemental maps clearly confirm the presence of potassium (K), strontium (Sr), and copper (Cu) from the respective metal salts, along with carbon (C), nitrogen (N), and oxygen (O) originating within the synthesized pyrotechnic formulations and their EDX weight ratios are given in Supporting Information. The EDX results affirm the successful incorporation of the metal salts into the nitrogen-rich fuel matrix, indicating effective blending of the metal oxidizers with compound **2** and binder matrix of the pyrotechnic formulation.

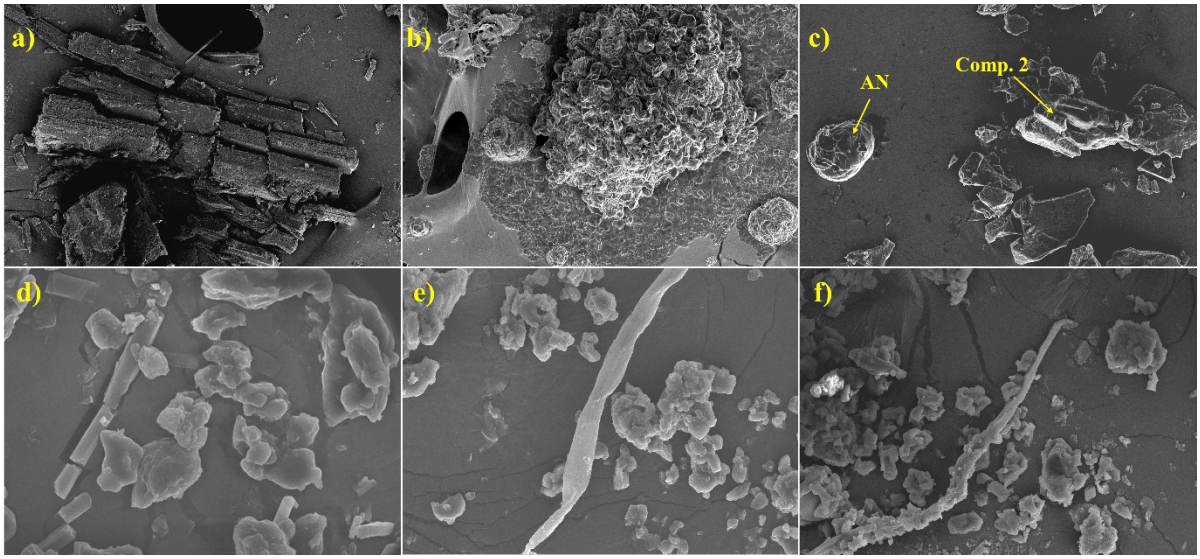

Figure S13. SEM image of (a) Compound **2** b) AN c) Formulation between compound **2** and AN (d) Pyrotechnic Formulation 1 (e) Pyrotechnic Formulation 2 (f) Pyrotechnic Formulation 3.

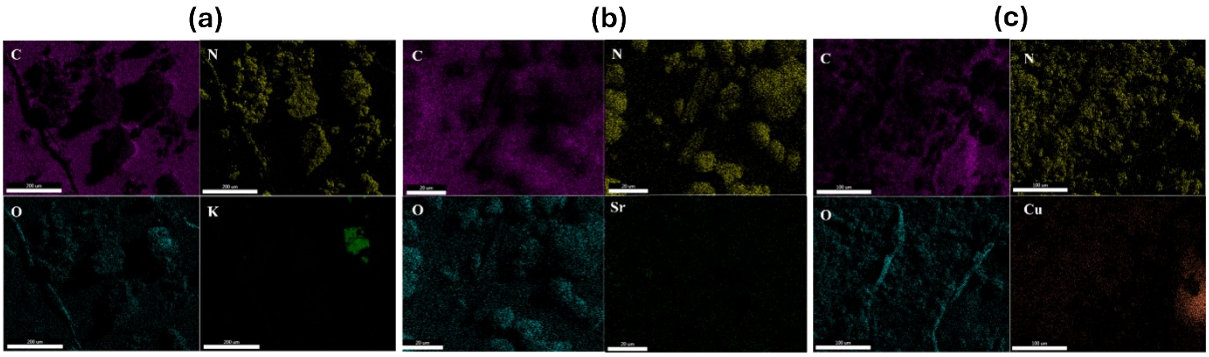

Figure S14. EDS mapping of (a) Pyrotechnic Formulation 1 (b) Pyrotechnic Formulation 2 (c) Pyrotechnic Formulation 3.

EDX data of Pyrotechnic Formulations:

1) **Pyrotechnic Formulation 1**

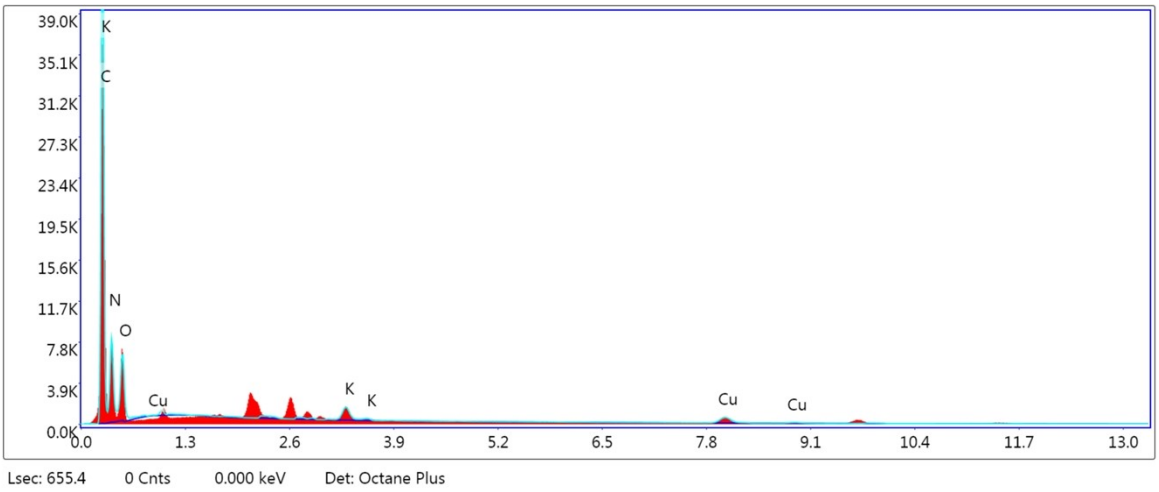

Pyrotechnic Formulation	C		N		O		K	
	Weight (%)	Atomic (%)	Weight (%)	Atomic (%)	Weight (%)	Atomic (%)	Weight (%)	Atomic (%)
1	65.16	70.39	24.52	22.71	7.71	6.25	0.87	0.29

2) Pyrotechnic Formulation 2

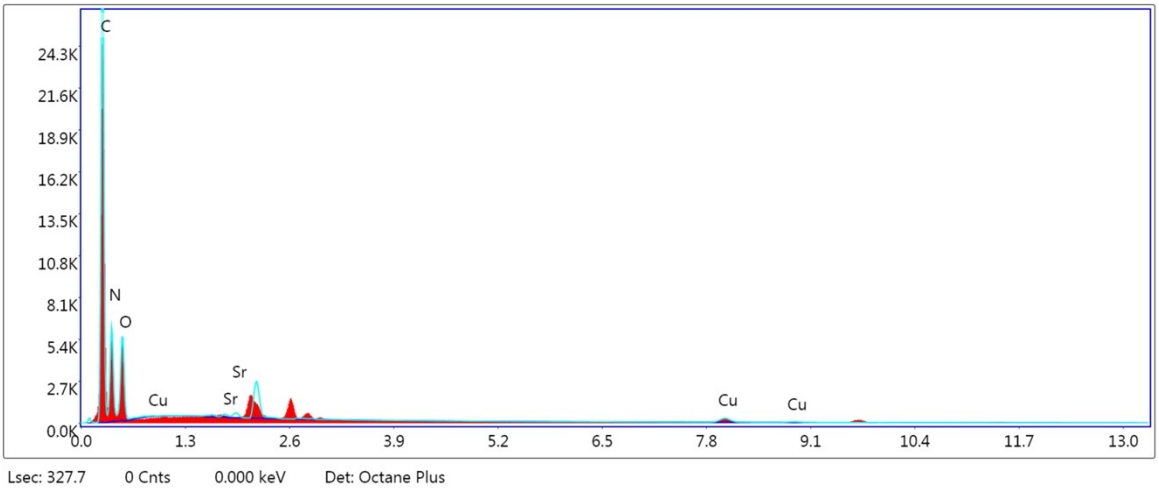

Pyrotechnic Formulation	C		N		O		Sr	
	Weight (%)	Atomic (%)	Weight (%)	Atomic (%)	Weight (%)	Atomic (%)	Weight (%)	Atomic (%)
2	59.07	65.66	26.54	25.30	9.90	8.26	2.81	0.43

3) Pyrotechnic Formulation 3

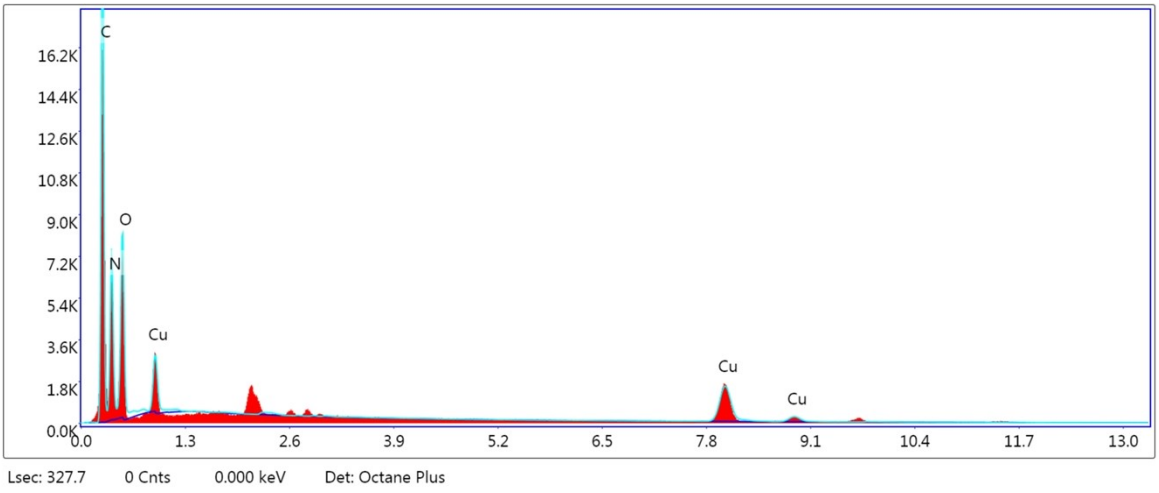

Pyrotechnic Formulation	C		N		O		Cu	
	Weight (%)	Atomic (%)	Weight (%)	Atomic (%)	Weight (%)	Atomic (%)	Weight (%)	Atomic (%)

3	41.63	50.70	31.01	32.38	15.54	14.21	11.81	2.72

Stability of the Pyrotechnic Formulations

In order to robustly evaluate the long-term chemical stability and potential interactions of compound **2** and the nitrate-based oxidizers (potassium nitrate, strontium nitrate and copper nitrate), a vacuum–thermal stability assessment was performed using an in-house high-vacuum system. The pyrotechnic formulations were heated at 70 °C under reduced pressure for 8 h. Fourier-transform infrared (FT-IR) spectra were recorded before and after the vacuum–thermal treatment. The post-treatment spectra were essentially identical to the corresponding pre-treatment spectra, with no appearance, disappearance, or shift of characteristic absorption bands as depicted in **Figures S15- S17**. These results indicate that compound **2** remains chemically stable and does not undergo degradation under prolonged thermal exposure in vacuum conditions.

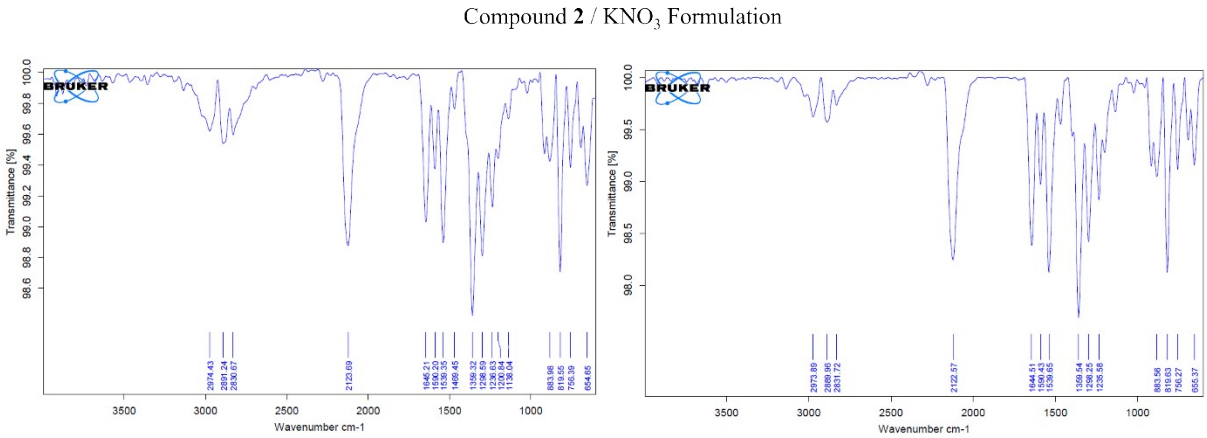

Figure S15. IR spectra of compound **2** / KNO_3 formulation before and after the vacuum-thermal treatment.

Compound **2** / Sr $(NO_{3)2}$ Formulation

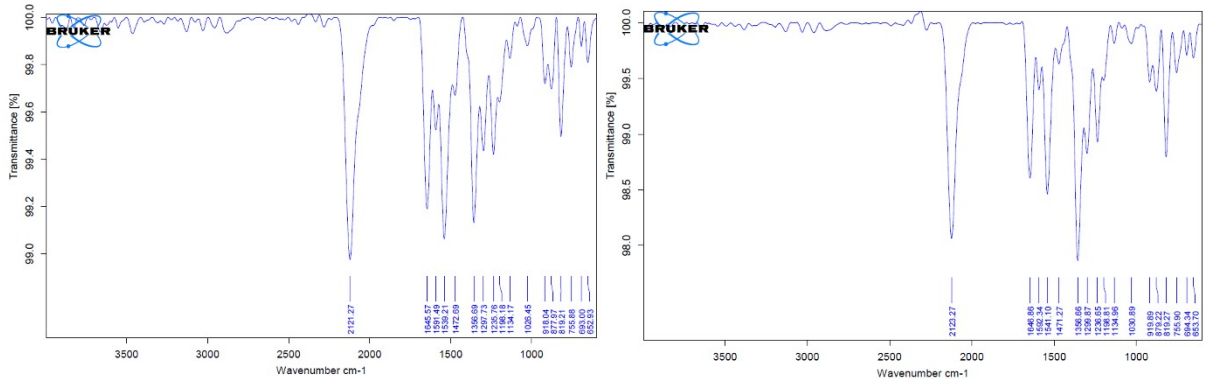

Before vacuum- thermal treatment

After vacuum- thermal treatment

Figure S16. IR spectra of compound **2** / Sr $(NO_3)_2$ formulation before and after the vacuum-thermal treatment.

Compound **2** / Cu $(NO_{3)2}$ Formulation

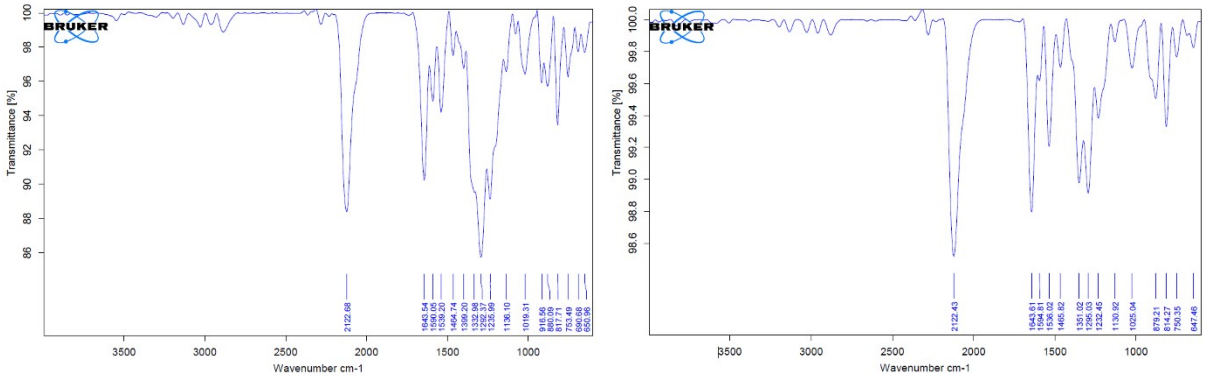

Before vacuum- thermal treatment

After vacuum- thermal treatment

Figure S17. IR spectra of compound **2** / Cu $(NO_3)_2$ formulation before and after the vacuum-thermal treatment.

Computational details

Computations were carried out using the Gaussian 09 program suite.[6] The structure optimizations are performed with B3LYP functional with 6-311G (d,p) basis set and characterized to be true local energy minima on the potential energy surface and no imaginary frequencies were found. Isodesmic reactions have been designed to predict the gas phase HOF (HOF_{gas}) and shown in **Figure S18**. The total energies (E_0), zero-point correction (ZPE), thermal corrections (H_T), and the experimental/calculated HOF values of the reference compounds used in isodesmic reactions and other derivatives are given in **Tables S6**. The usage of HOF_{gas} in the calculation of detonation properties slightly overestimates the values of detonation velocity and detonation pressure, and hence, the solid phase HOF (HOF_{solid}) can

effectively reduce the errors. The HOF_{solid} is calculated as the difference between HOF_{gas} and heat of sublimation (HOF_{sub}) as,

$$HOF_{solid} = HOF_{gas} - HOF_{sub} \quad (1)$$

HOF_{sub} depend on the molecular surface properties and calculated using equation (2) proposed by Politzer et al.[7],

$$HOF_{sub} = 4.4307\ x\ 10^{-4}A^2 + 2.0599\left(v\sigma_{tot}^2\right)^{0.5} - 2.4825 \quad (2)$$

where A represent the surface area of the 0.001 electrons/bohr^4 isosurface of electronic density, v denotes the degree of balance between the positive and negative surface potentials, and σ_{tot}^2 is the electrostatic potential variance. The molecular surface properties (see **Table S7**) were obtained using the Multiwfn program[8].

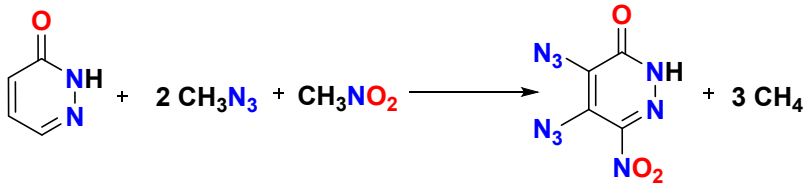

Figure S18: Designed isodesmic reaction for the prediction of HOF_{gas} for compound **2.**

Table S6: Calculated total energies at 298K (E_0), zero-point energies (ZPE), and thermal corrections (H_T) and HOF_{gas} of reference and target compounds at the B3LYP/6-311G(d,p) level.

Compd.	**E_0 (a.u.)**	**ZPE (au)**	**H_T (au)**	**HOF_{gas} (kJ/mol)**
	-339.535884	0.081504	0.006094	45.05
CH_3N_3	-204.092833	0.05015	0.005418	293.91
CH_3NO_2	-244.866526	0.0502	0.0053	-81
CH_4	-40.485334	0.0446	0.00381	-74.8

Table S7: Calculated molecular surface properties and heat of sublimation of target compounds.

Compd.	**Surface area ($Å^2$)**	**Volume ($Å^3$)**	σ_{tot}^2 **(kcal/ mol)^2**	**v**	**HOF_{Sub} (kJ/mol)**	**HOF_{Gas} (kJ/mol)**
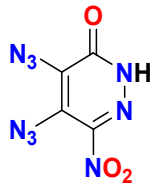	209.73130	209.52012	175.32238	0.24366470	106.73	326.76

References:

1) G. M, Sheldrick, *Acta Cryst.* 2008, **A64**, 339-341.
2) O. V. Dolomanov, L. J. Bourhis, R. J. Gildea, J. A. K. Howard and H. Puschmann, *J. Appl. Crystallogr.* 2009, **42**, 339-341**.**
3) G. M. Sheldrick, *Acta Crystallogr. Sect. A Found. Adv.* 2015, **71**, 3-8.
4) G. H. Sung, B. R. Kim, K. E. Ryu and Y. J. Yoon, *J. Korean Chem. Soc.* 2014, **58**, 140.
5) T. M. Klapötke and M. Suceska *Z. Anorg. Allg. Chem.* 2021, **647**, 572 – 574.
6) M. J. Frisch, G. W. Trucks, H. B. Schlegel, *et al. Gaussian 09, Revision B. 01;* Gaussian, Inc.: Wallingford, 2013.
7) P. Politzer, Y. Ma, P. Lane and M. C. Concha, *Int. J. Quantum Chem.* 2005, **105**, 341.
8) T. Lu and F. Chen, *J. Comput. Chem.* 2012, **33**, 580.